FRA-OR&D 75-16

THE AERODYNAMIC ANALYSIS OF SINGLE AND MULTIPLE VEHICLES

CHARLES R. STROM Ph. D.

JANUARY 1975

TECHNICAL REPORT

Document is available to the public
through the National Technical
Information Service, Springfield, Virginia 22151

Prepared for

FEDERAL RAILROAD ADMINISTRATION
Office of Research and Development
Washington, D.C.

TECHNICAL REPORT STANDARD TITLE PAGE

1. Report No.	2. Government Accession No.	3. Recipient's Catalog No.
FRA-ORD & D 75-16		PB 244 068

4. Title and Subtitle	5. Report Date
THE AERODYNAMIC ANALYSIS OF SINGLE AND MULTIPLE VEHICLES ENTERING AND TRAVELING IN OPEN TUNNELS	January 1975
	6. Performing Organization Code

7. Author(s)	8. Performing Organization Report No.
Charles R. Strom Ph.D.	MTR-6755

9. Performing Organization Name and Address	10. Work Unit No.
The MITRE Corporation, Westgate Park, McLean, VA	11. Contract or Grant No. DOT-FR-54090
	13. Type of Report and Period Covered
12. Sponsoring Agency Name and Address Office of Research, Development and Demonstration Federal Railroad Administration 2100 2nd Street, S.W. Washington, D.C. 20590	Technical Report
	14. Sponsoring Agency Code

15. Supplementary Notes

16. Abstract

The analyses required to calculate the aerodynamic effects of tunnel entry, tunnel venting and multiple vehicle motions in open ended tunnels are presented. Results for several cases of open ended tunnel travel and various entry configurations are presented and described. The effects of an earlier vehicle's motion on the pressure peak associated with a second vehicle entering a tunnel are presented and discussed.

PRICES SUBJECT TO CHANGE

17. Key Words	18. Distribution Statement
Aerodynamic Effects, Tunnel Entry, Tunnel Venting	Document is available to the public through National Technical Information Service, Springfield, VA 22151

19. Security Classif. (of this report)	20. Security Classif. (of this page)	21. No. of Pages	22. Price PC/MF
Unclassified	Unclassified	46	$3.75/2.25

Form DOT F 1700.7 (8-69)

TABLE OF CONTENTS

LIST OF ILLUSTRATIONS

LIST OF ILLUSTRATIONS
(Cont'd)

NOMENCLATURE

A	local area
C_D	drag coefficient defined in terms of maximum vehicle velocity
c	speed of sound
D	tunnel diameter
d	vehicle diameter
F_1	tunnel friction term (unsteady)
F_2	vehicle friction term (unsteady)
F_3	tunnel friction term (steady)
F_4	vehicle friction term (steady)
L	tunnel length
ℓ	vehicle length
p	static pressure
p_o	stagnation pressure
Q	volumentric flow rate through wall.
Q'	near field volumetric flow rate
q_1	rate of heat transfer from tunnel wall (unsteady)
q_2	rate of heat transfer from vehicle wall (unsteady)
q_3	rate of heat transfer from tunnel wall (steady)
q_4	rate of heat transfer from vehicle wall (steady)
R	gas constant
R'	defined by Equation 5
Re	Reynolds number
T	temperature

t time

u gas velocity relative to tunnel

V vehicle velocity

w gas velocity relative to vehicle

x distance coordinate from entrance of tunnel

x_v instantaneous length of vehicle (inside tunnel during entry)

β blockage ratio

γ ratio of specific heats

Δt change in time coordinate

Δx change in x-coordinate

κ discharge coefficient for tunnel venting

ρ density

τ frictional force

Subscriptions

a = approach condition at vehicle nose

T = tunnel

v = vehicle

x = approach conditions to shock

y = conditions behind shock

Superscripts

$*$ = sonic point conditions

1.0 INTRODUCTION

This report presents the recent results of a continuing series of studies at The MITRE Corporation on the aerodynamics of vehicles traveling in tunnels. An earlier report (Reference 1) documented the details of the present theoretical/numerical approach and included several numerical examples of vehicles traveling in closed-ended tunnels, neglecting heat transfer effects.

The extensions to this previous work included here are: travel in open tunnels with heat transfer; tunnel entry, including the effects of variable area geometry and venting at the entrance section; the effects of multiple, independent vehicle motions in a single tunnel, and the effects of tunnel wall venting along the length of the tunnel.

The purpose of this report is to present the extensions to the analyses given earlier (Reference 1) which are required in order to calculate the open tunnel and entry problem described above. Included also are several computational results for open tunnel travel and tunnel entry. These results, used in conjunction with the closed-ended results of Reference 1, can be used to estimate preliminary design requirements for a wide range of operating conditions. Unfortunately, while the changes required to include the effects of tunnel venting have been incorporated into the current version of the computer program, there was insufficient time available to calculate useful tunnel venting results. Therefore, presentation of these results must await completion of further computational studies.

2.0 ANALYSIS

The analysis required to extend the previous work (Reference 1) to include the effects of heat transfer, venting and tunnel entry are presented in this section. As the methodology used is very similar to that presented earlier, little detail is provided here. Comparison with the detailed descriptions provided in Reference 1 will yield the appropriate modifications which were included here.

2.1 Far Field Analysis

The equations used for the unsteady far-field calculation are very similar to those presented earlier. Again, a finite difference analogue, based upon MacCormack's method, is used to integrate the one-dimensional, unsteady, compressible flow equations with area changes, heat transfer, mass transfer and skin friction effects included (Reference 2). Written in a tunnel-fixed coordinate system (Figure 1) the far-field equations are:

(continuity) $$\frac{\partial \rho}{\partial t} + \rho \frac{\partial u}{\partial x} + u \frac{\partial \rho}{\partial x} + \frac{\rho u}{A}\left(\frac{dA}{dx}\right) = - \frac{\rho Q}{A} \qquad (1)$$

(momentum) $$\frac{\partial u}{\partial t} + u \frac{\partial u}{\partial x} + \frac{1}{\rho} \frac{\partial p}{\partial x} + F_1 + \frac{Qu}{A} = 0 \qquad (2)$$

(energy) $$\frac{\partial p}{\partial t} + u \frac{\partial p}{\partial x} - c^2 \left(\frac{\partial \rho}{\partial t} + u \frac{\partial \rho}{\partial z}\right) = (\gamma-1)\rho\,(-q_1 + uF_1) \qquad (3)$$

(state) $$p = \rho RT \qquad (4)$$

where, area change and mass transfer are included in equations (1), (2) and (3). Here, ρQ is the mass flow rate through a unit length of the tunnel wall (positive = inflow). It is further assumed that the flow through the walls has no axial component of velocity. The solution method and nomenclature are similar to those described in Reference 1.

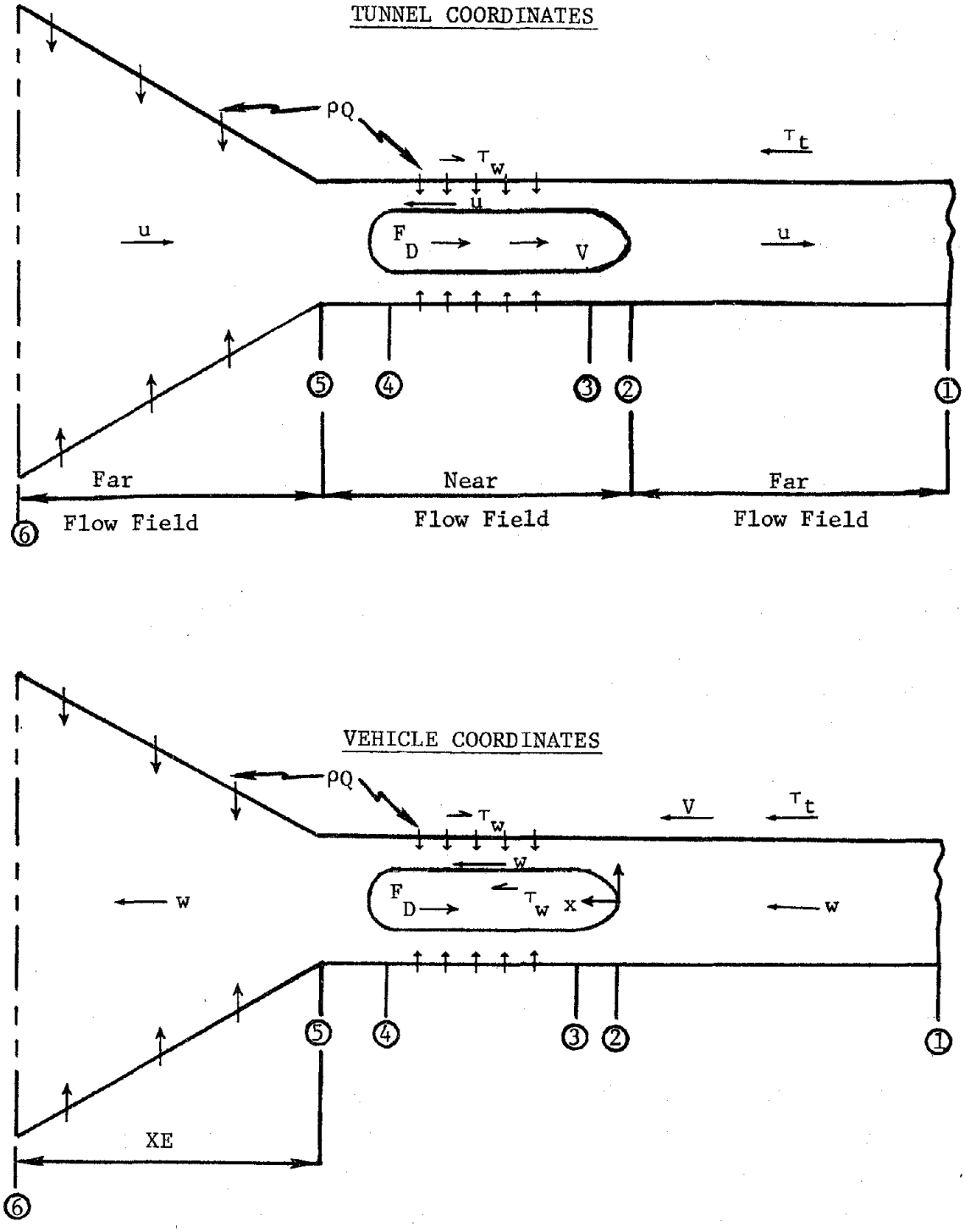

FIGURE 1
LABORATORY AND MOVING COORDINATES FOR
VEHICLE IN VENTED TUBE

An additional simplification is introduced in order to solve the venting problem. First, for each time step, t, the far-field solution is obtained from the previous step assuming no venting. Then, the venting is assumed concentrated at each computational node point. The amount of venting is calculated using Bernoulli's equation where,

$$R' = \kappa \sqrt{\frac{2(p-p_{ATM})}{\rho}} \quad \frac{(p-p_{ATM})}{|p-p_{ATM}|} \tag{5}$$

and

$$Q = \alpha A_{ref} R' \tag{6}$$

here, A_{ref} is the surface area of the tunnel wall appropriate to the current computation node point, α is an input constant, defining the percent venting, and κ is the discharge coefficient for the tunnel vents. Utlizing this flow out of the tunnel, the continuity equation (Equation 1) is used to provide a new flow velocity at the given computational point. This procedure is used for each point in the far-field.

2.2 The Near-Field Solution

Utilizing the nomenclature of Section 2.3 of Reference 1, the near-field equations become:

$$\frac{\rho w}{A}\frac{dA}{dx} + \rho \frac{dw}{dx} + w \frac{d\rho}{dx} = -\frac{\rho Q'}{A} \tag{7}$$

$$\frac{wdw}{dx} + \frac{1}{\rho}\frac{dp}{dx} + F_3 + F_4 + \frac{Q'w}{A} = 0 \tag{8}$$

$$w\frac{dp}{dx} - c^2 w \frac{d\rho}{dx} = (\gamma-1)\rho(q_3 + q_4 + w(F_3 + F_4) + V F_3) \tag{9}$$

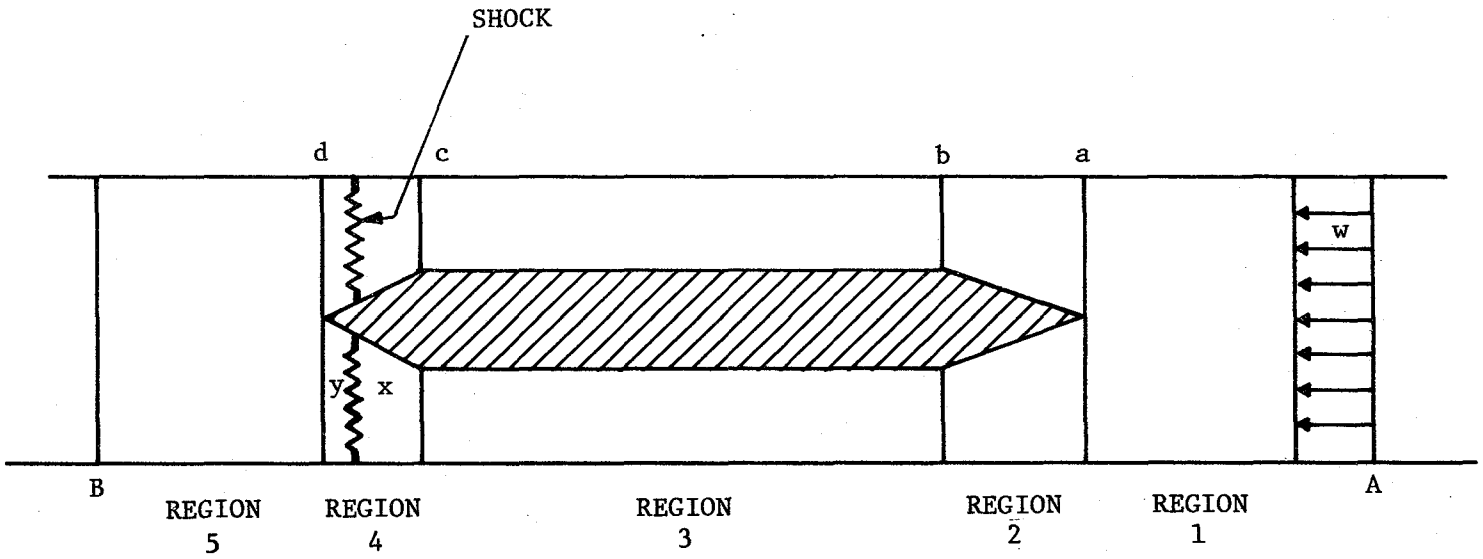

FIGURE 2
SEPARATE INTEGRATION REGIONS FOR NEAR-FIELD SOLUTIONS

where $\rho Q'$ is the mass rate of flow though a unit length of the tunnel/annulus walls. The method of solution of these equations is exactly as described in Reference 1 for Regions 1, 2, 4 and 5, (Figure 2). However, the equations in the annulus region (Region 3) are integrated in a step-by-step fashion in order to include heat and mass transfer.

Heat transfer is calculated by using the Reynolds analogy at each computational point (Reference 1). Mass flow in the near-field solution is calculated in a manner similar to that described above for the far-flow field solution.

2.3 Tunnel-entry

Several simplifications are introduced into the tunnel entry calculations in order to simplify the boundary condition matching procedure at the rear of the vehicle.

The drag on that portion of the vehicle external to the tunnel is neglected. The vehicle is replaced by one of increasing length, whose instantaneous length is (See Figure 3):

$$x_v = V(t - t_I) \tag{10}$$

where t = time since vehicle has entered tunnel

t_I = time vehicle begins entering tunnel

and V = velocity of vehicle.

The procedure used to obtain the flow parameters at each computational step at the nose of the vehicle is the same as that described in the matching problem in Reference 1, except that until the vehicle completely enters the tunnel, the pressure ahead of the vehicle is adjusted for each computational step until the pressure at the rear annulus is equal to the atmospheric pressure at the tunnel entrance, or a preset fraction thereof.

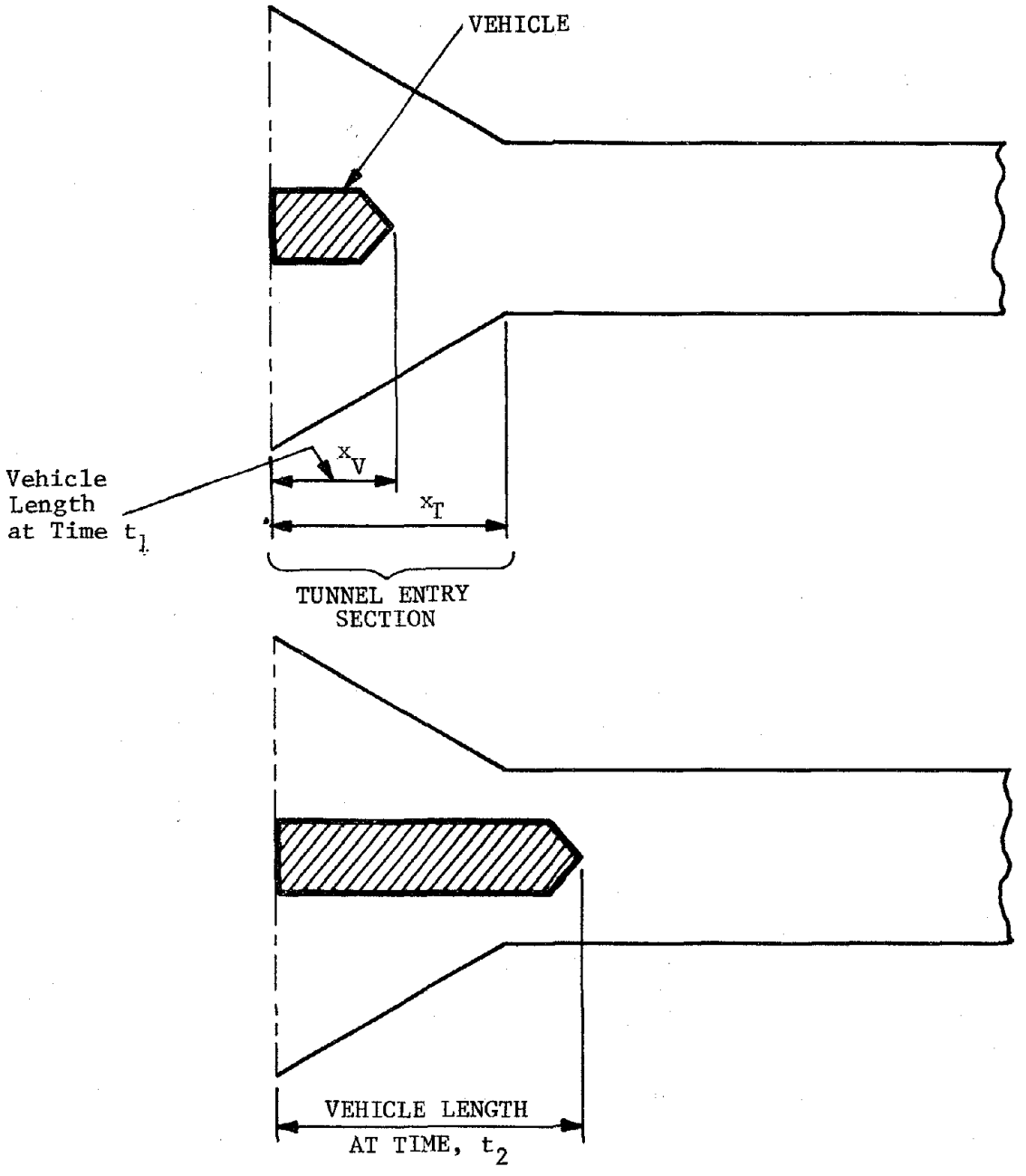

FIGURE 3
TUNNEL ENTRY

If the vehicle enters a flared entrance, the equivalent blockage at each point along the flared section is calculated using the position of the vehicle and the shape of the flare. (To date only straight sided flares have been considered.) The computations then proceed exactly as previously described (Reference 1) for the near-field solution.

2.4 Multiple-Vehicle Operation

There are several types of multiple vehicle operations which can readily be calculated using the present program. These include two or more vehicles traveling in the same or opposite directions, although passing vehicles cannot be accounted for. The difficulty imposed by multiple vehicle operation is that of computer run times associated with the bookkeeping of following more than one near-field (i.e. vehicle). Consequently, only the simplest case of multiple vehicle motion has been considered here. This is the case where a very long time after one vehicle has entered a tunnel, another vehicle of the same length then enters the same tunnel at the same speed. The effects of the first vehicle's motion on the second are considered.

3.0 RESULTS

Several results have been calculated using the present MITRE computer program. These include open tunnel computations under a wide range of tunnel geometry and vehicle operating conditions; tunnel entry in straight walled tunnels; tunnel entry in flared tunnels; and one-way multiple vehicle operations. Venting has not been included due to lack of sufficient time to complete the computations. The equations and procedures required to perform venting calculations have been incorporated into the computer program however. Hopefully these computations can be reported in the near future.

3.1 Open Tunnel Results

3.1.1 Blockage Ratio Effects

Figures 4 through 10 present the effects of blockage ratio on the drag and flow parameters for a vehicle ℓ/d ratio of 30, a tunnel L/D ratio of 10000 and a vehicle velocity, V = 440 fps. The computations were performed for a vehicle diameter d = 10 ft. The tunnels were open ended. As can be seen, the effects of the tunnel ends are more pronounced as the length of the tunnel decreases. The effects shown are not unusual, indicating that for the shorter tunnels it will be very important to have available an unsteady computation method in order to properly assess the drag and power requirements. The physics of the flow fields associated with these runs are not unlike those described for closed tunnels in Reference 1 and will not be discussed here. The accuracy of the method for open tunnels has been verified in Reference 3.

3.1.2 Vehicle ℓ/d Ratio Effects

The effects of increasing vehicle ℓ/d ratio are shown in Figures 11 through 17. As shown in Figures 11 through 13, the increase in vehicle length causes a proportional increase in drag through both a pressure increase in the nose region and a pressure decrease in the tail region. Vehicle ℓ/d effects are much less severe than blockage effects and can be readily estimated for a wide range of problems from the accompanying curves.

3.1.3 Effects of Tunnel L/D Ratio

The drag and flow parameters are shown in Figures 18 through 24 for various tunnel L/D ratios. As can be seen, for open tunnels, the tunnel length can have a significant effect on the drag and must be fully accounted for. For very long tunnels, the effect of changing tunnel length is apparently less significant.

3.2 Tunnel Entry

3.2.1 Straight Walled Entry Section

The pressure distribution in front of a vehicle entering a tunnel at a velocity, V = 164 ft/sec is shown in Figure 25. Also shown are similar results from Reference 2. In this comparison, two points should be noted. First, the peak pressure of the initial wave in the MITRE computation is lower than that of Reference 2. This is probably not too significant and can be attributed to the use of slightly different loss coefficients and skin friction coefficients in the near flow field region. Similar discrepencies were noted in Reference 1 when comparing data to experimental results. Of more significance is the lack of resolution of the pressure peaks for the reflected

waves in the MITRE results as the vehicle passes along the tunnel. This can probably be attributed to the numerical finite difference procedure which would tend to smear out pressure waves as the computations proceed with time. This will only cause design problems when great detail is desired for the pressure pulses near the body. In this case, greater resolution could be obtained by using a finer spatial mesh in the MITRE program.

Referring to Figure 25, the following points can be noted. As the train enters, the pressure rises sharply because air is accelerated both along the tunnel and out the entrance portal. The pressure then continues to rise, though more gradually, as the frictional pressure drop in the annulus increases.

After about 2 sec., the pressure reduces because the rear of the vehicle has entered the tunnel. At about 3 sec., a much larger reduction occurs when the first reflection of the primary wave arrives. The subsequent reflection of this rarefaction wave causes a new compression wave to travel along the tunnel. The pressure at the nose therefore rises again (4 1/2 sec.) and it rises further when the reflection of the rarefaction wave generated by the rear of the train arrives from the opposite end of the tunnel (5 1/2 sec.). This process repeats as the vehicle traverses the tunnel.

As can be seen in Figure 25, if the magnitude of the initial pressure wave can be decreased, the environment within the vehicle would be similarly affected. Thus, for passenger comfort, methods to decrease the magnitude of this initial pressure wave should be investigated. Amoung the obvious choices for accomplishing this decrease for a given blockage are; venting, flared entrances, and flow preconditioning.

3.2.2 Flared Entry

In Figure 25, the pressure history for a flared entry section (50 ft long) is compared to the equivalent straight walled solution. This solution was run primarily to check the computer program. As can be seen, the maximum pressure peak, while decreased, is not considerably altered. This result, which has been verified by previous investigators, indicates that to derive much benefit from a flared section, the section would most probably have to be long in comparison to the vehicle length. Such a flare may be expensive to build.

3.2.3 Multiple Vehicle Entry

The effect that one vehicle entering a tunnel has on a second similar vehicle which enters the same tunnel at a later time is shown in Figure 26. In this case, the first vehicle preconditions the flow in the tunnel so that the second vehicle is subjected to considerably less inertia loading from the tunnel flow. Consequently, the effect is to lower both the magnitude of the initial pressure pulse in front of the vehicle and also the rate of change of the growth of this pulse. Both effects could significantly improve passenger comfort. This result indicates that the initial pressure pulse can be greatly reduced by preconditioning the flow before a vehicle enters the tunnel. In most cases however, methods of attaining this result may again be expensive.

Tunnel venting, the final method to be studied for reducing the initial pressure pulse, will most likely yield the most successful results. Experimental evidence indicates that these primary pulses can be completely eliminated using adequate venting. Venting results await further study.

4.0 CONCLUSIONS

The MITRE program has been revised to include open tunnel travel, tunnel entry, flared entry sections, tunnel venting and multiple vehicle travel.

The results presented for open tunnels can be used to provide preliminary design data for drag and power requirements for a wide range of operating conditions and tube geometries.

The results presented for tunnel entry indicate that flared sections are probably too costly to be of much use in reducing the peak of the initial pressure pulse. Preconditioning of the flow in the tunnel would appear to be a more suitable alternative.

5.0 RECOMMENDATIONS

The MITRE program as developed should now be used to study tunnel venting and one-way multiple vehicle operations in tunnels. With additional modifications two way tunnel travel can also be investigated. Finally, tunnel exit should be added to the program so that a complete systems study of several vehicles entering and exiting a tunnel with venting effects included can be undertaken.

REFERENCES

1. Strom, C. A., Analytical Procedure for Calculating the Aerodynamic Performance of Vehicles Traveling in Tunnels, The MITRE Corporation Report No. MTR-6299, December 1972. FRA Report No. FRA-RT-73-14. PB 220 082

2. Fox, J. A. and Vardy, A. E., The Generation and Alleviation of Air Transients Caused by the High Speed Passage of Vehicles Through Tunnels, presented at the International Symposium on the Aerodynamics and Ventilation of Vehicle Tunnels, Canterbury, England, April 1973 (Paper No. G3).

3. Private Communication with A. Hammitt.

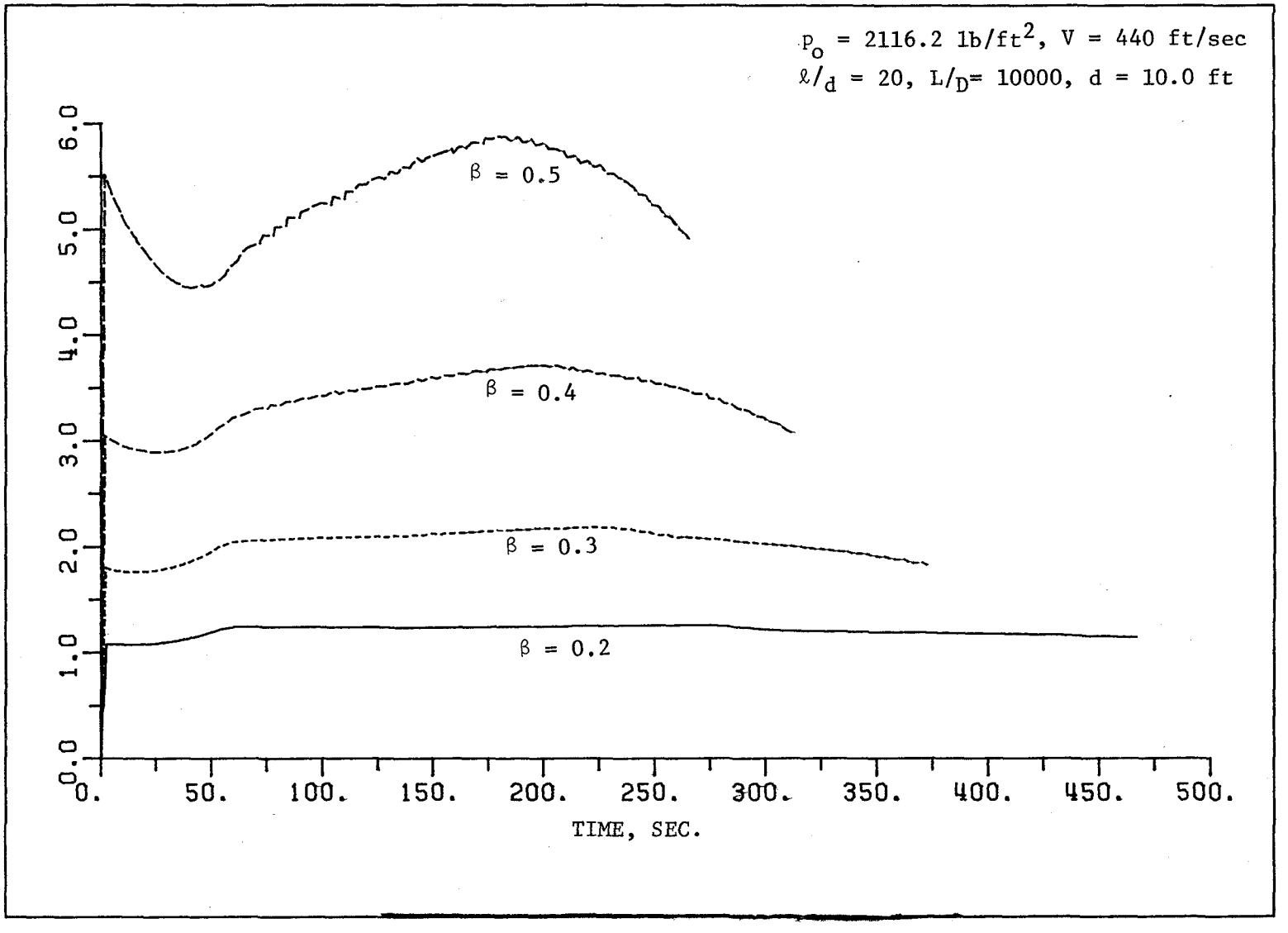

FIGURE 4

DRAG COEFFICIENT VS. TIME FOR VARIOUS

BLOCKAGE RATIOS, OPEN ENDED TUNNEL

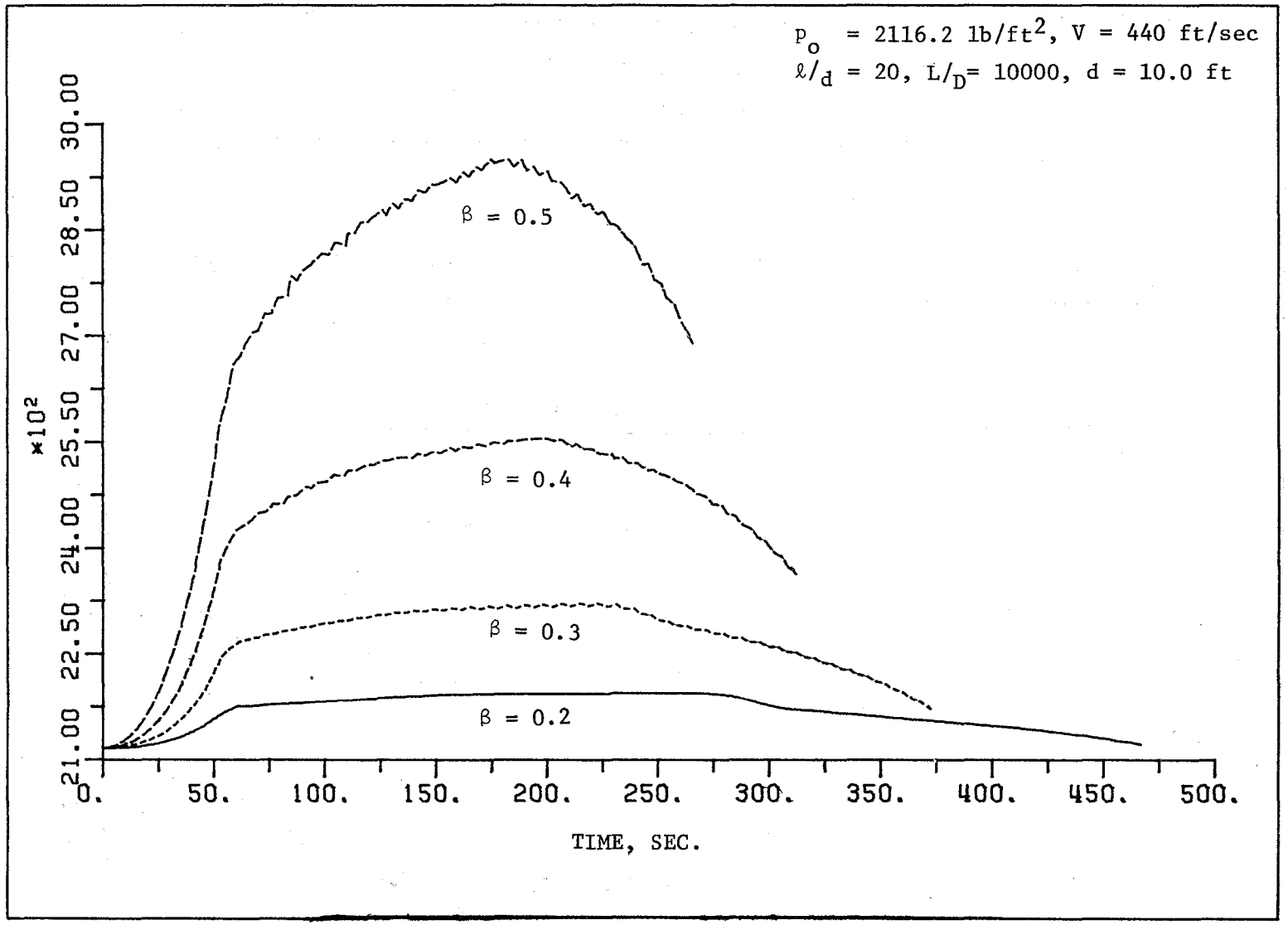

FIGURE 5

PRESSURE AT VEHICLE NOSE VS. TIME,

EFFECT OF BLOCKAGE RATIO

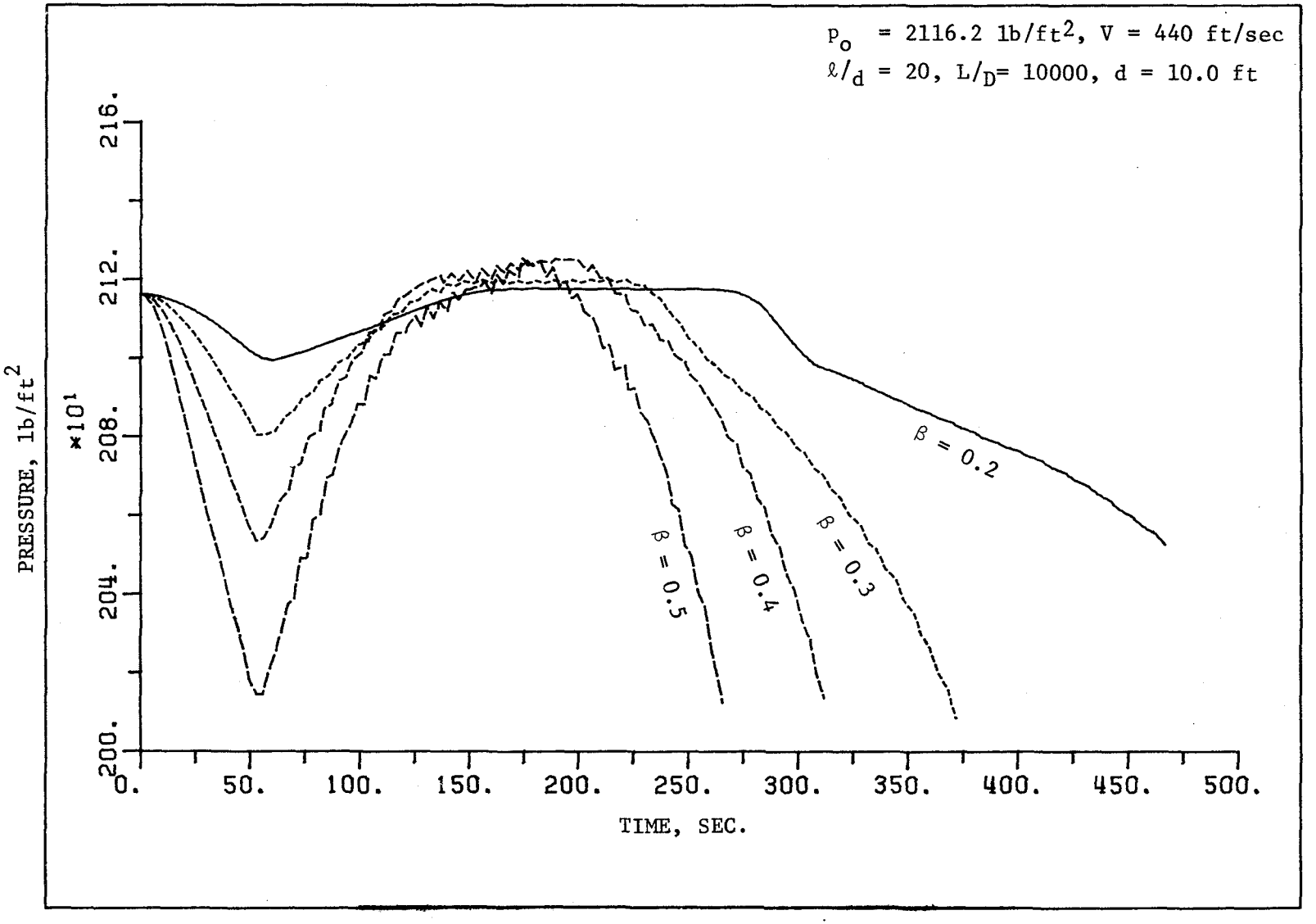

FIGURE 6

PRESSURE AT VEHICLE TAIL VS. TIME,

EFFECT OF BLOCKAGE RATIO

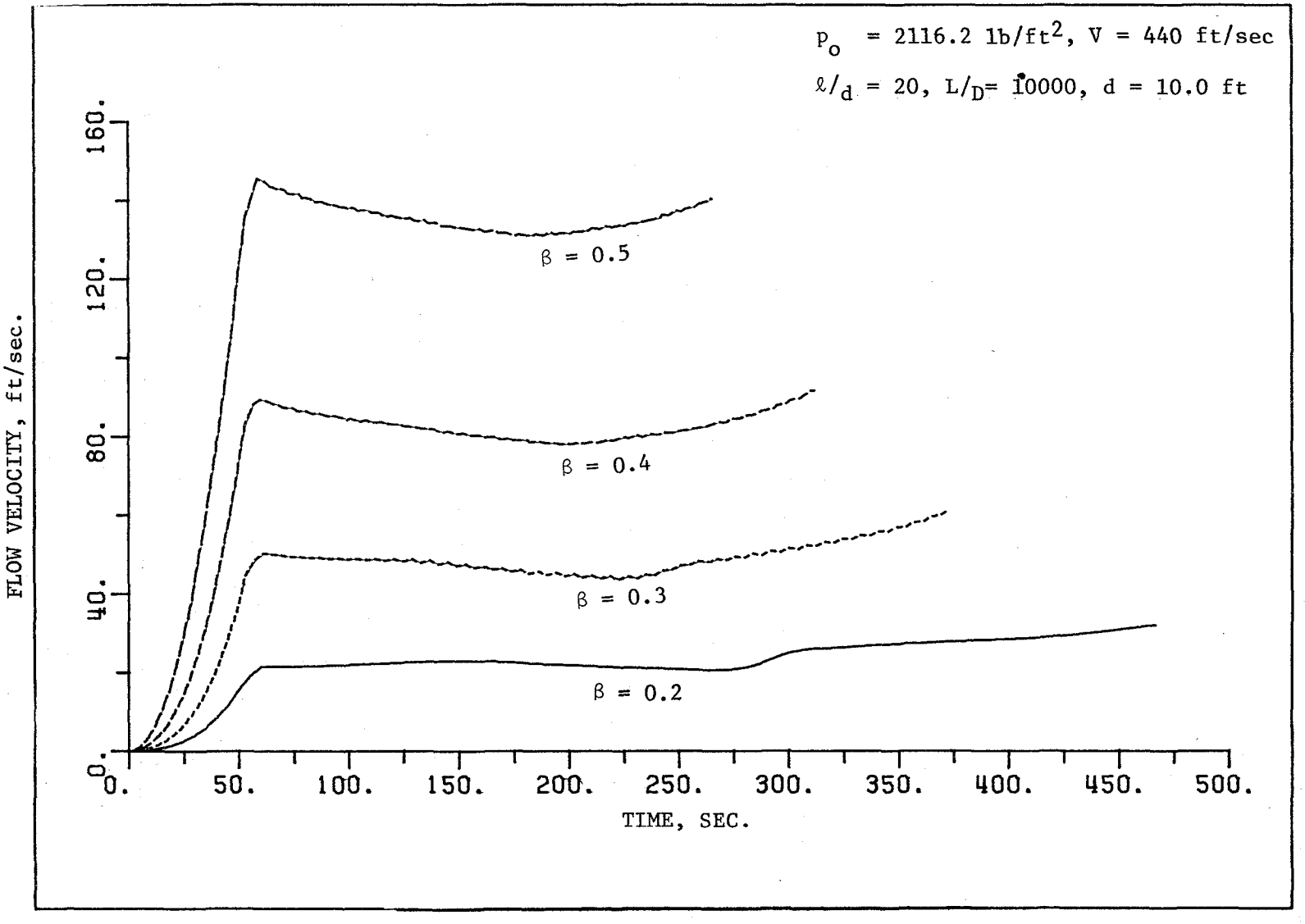

FIGURE 7

FLOW VELOCITY AT VEHICLE NOSE VS. TIME,

EFFECT OF BLOCKAGE RATIO

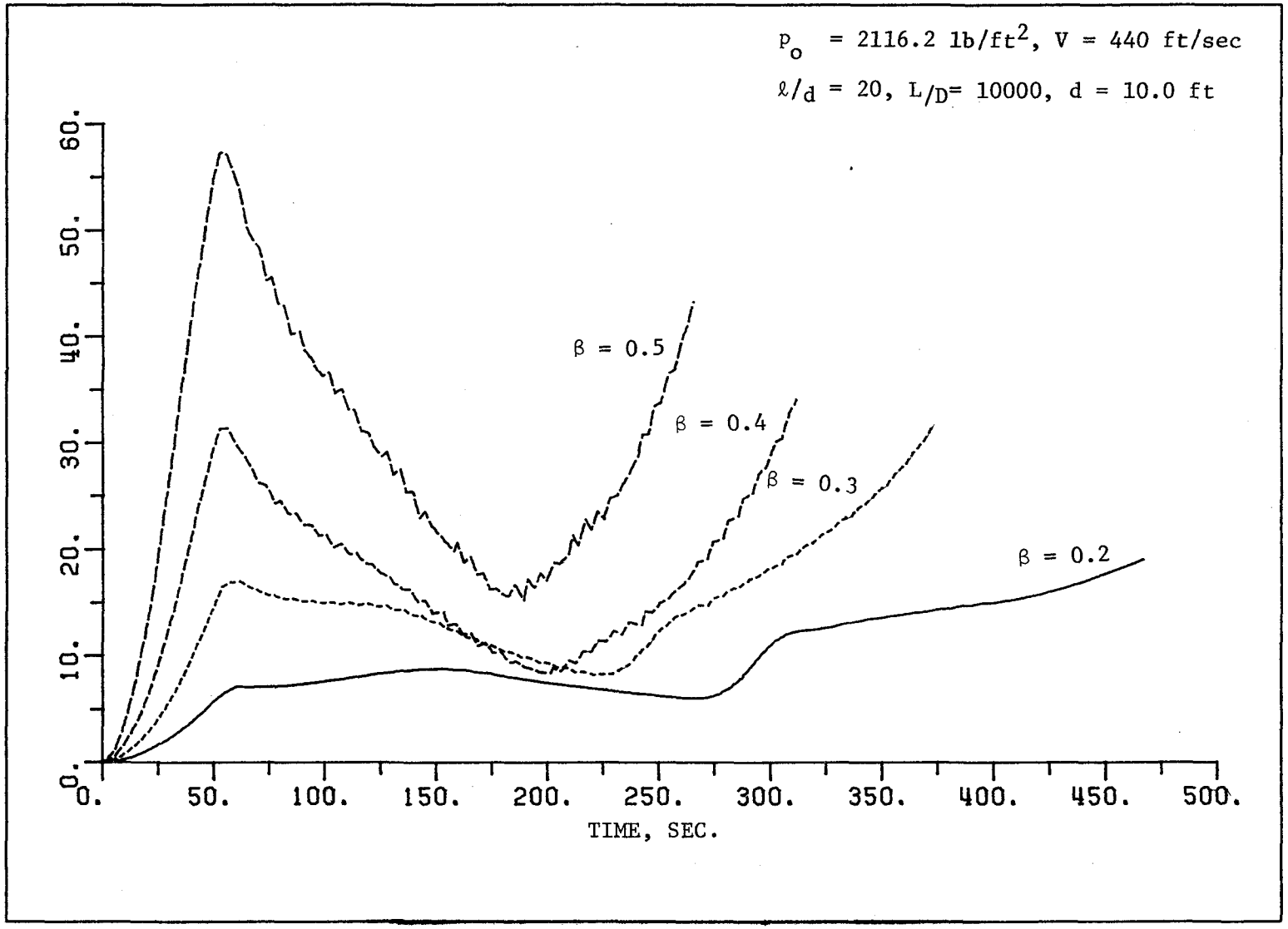

FIGURE 8

FLOW VELOCITY AT VEHICLE TAIL VS. TIME,

EFFECT OF BLOCKAGE RATIO

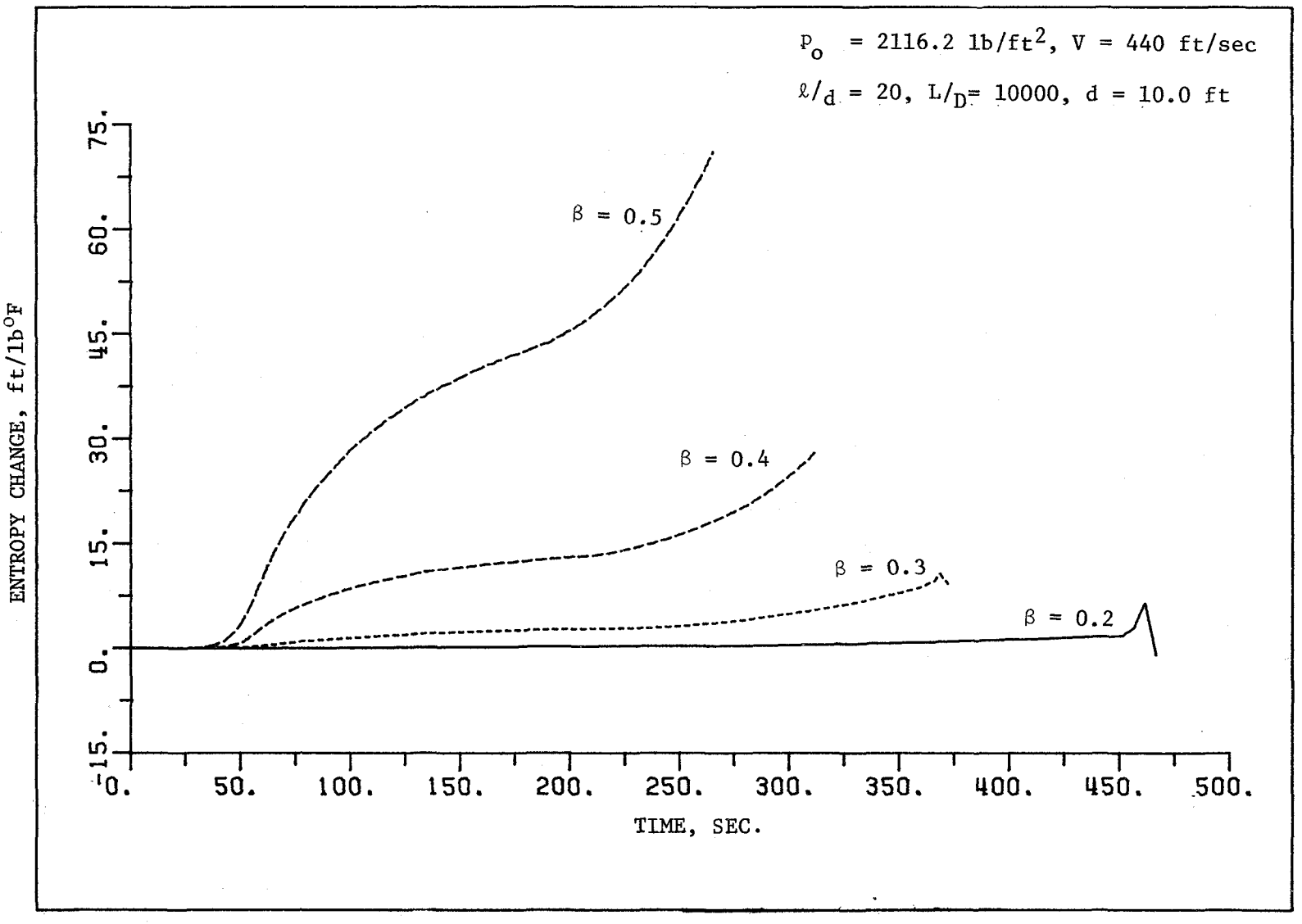

FIGURE 9

ENTROPHY CHANGE AT VEHICLE NOSE VS.

TIME, EFFECT OF BLOCKAGE RATIO

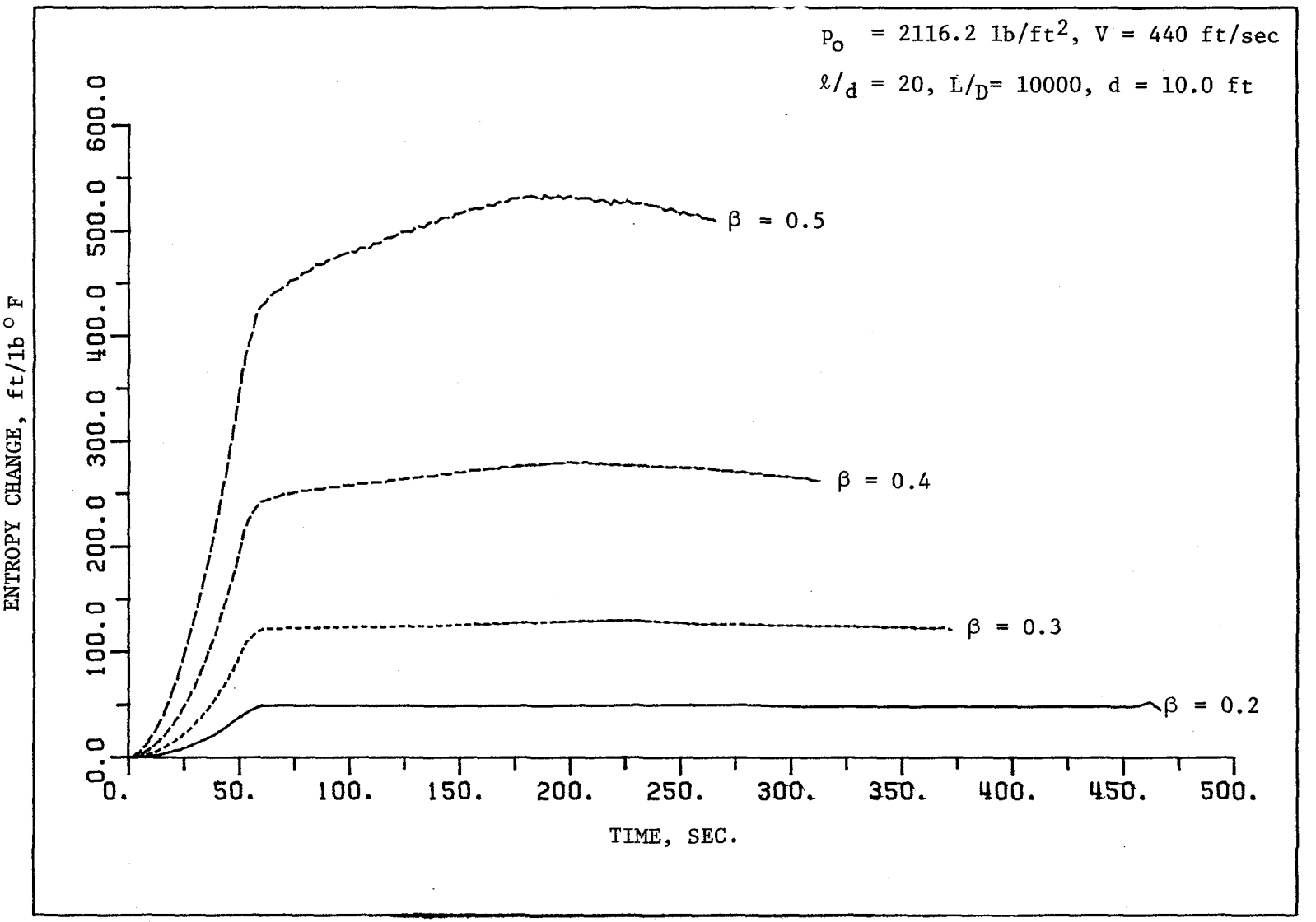

FIGURE 10

ENTROPHY CHANGE AT VEHICLE TAIL VS.

TIME, EFFECT OF BLOCKAGE RATIO

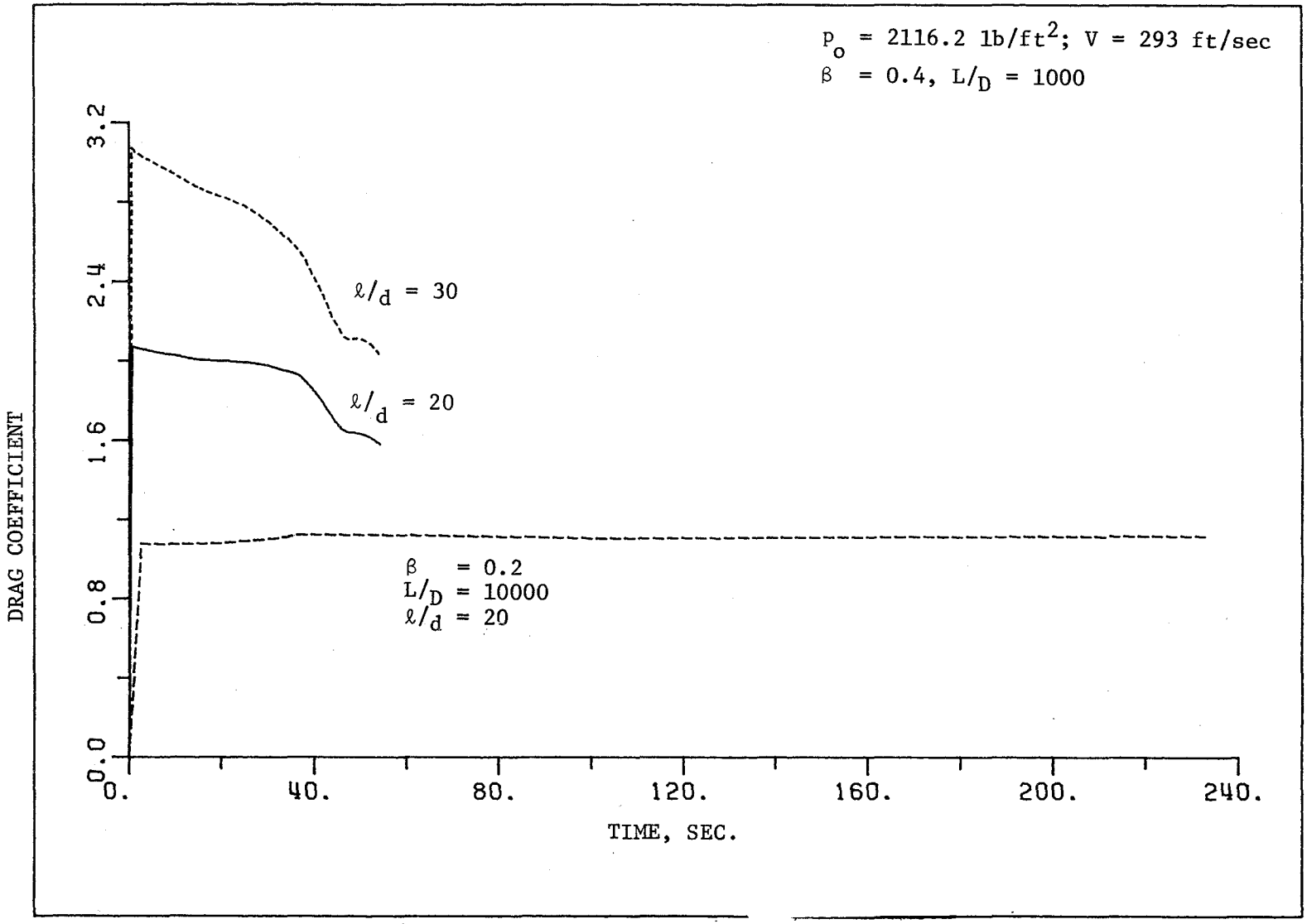

FIGURE 11

DRAG COEFFICIENT VS. TIME FOR VARIOUS VEHICLE $\ell/_d$ RATIOS, OPEN ENDED TUNNELS

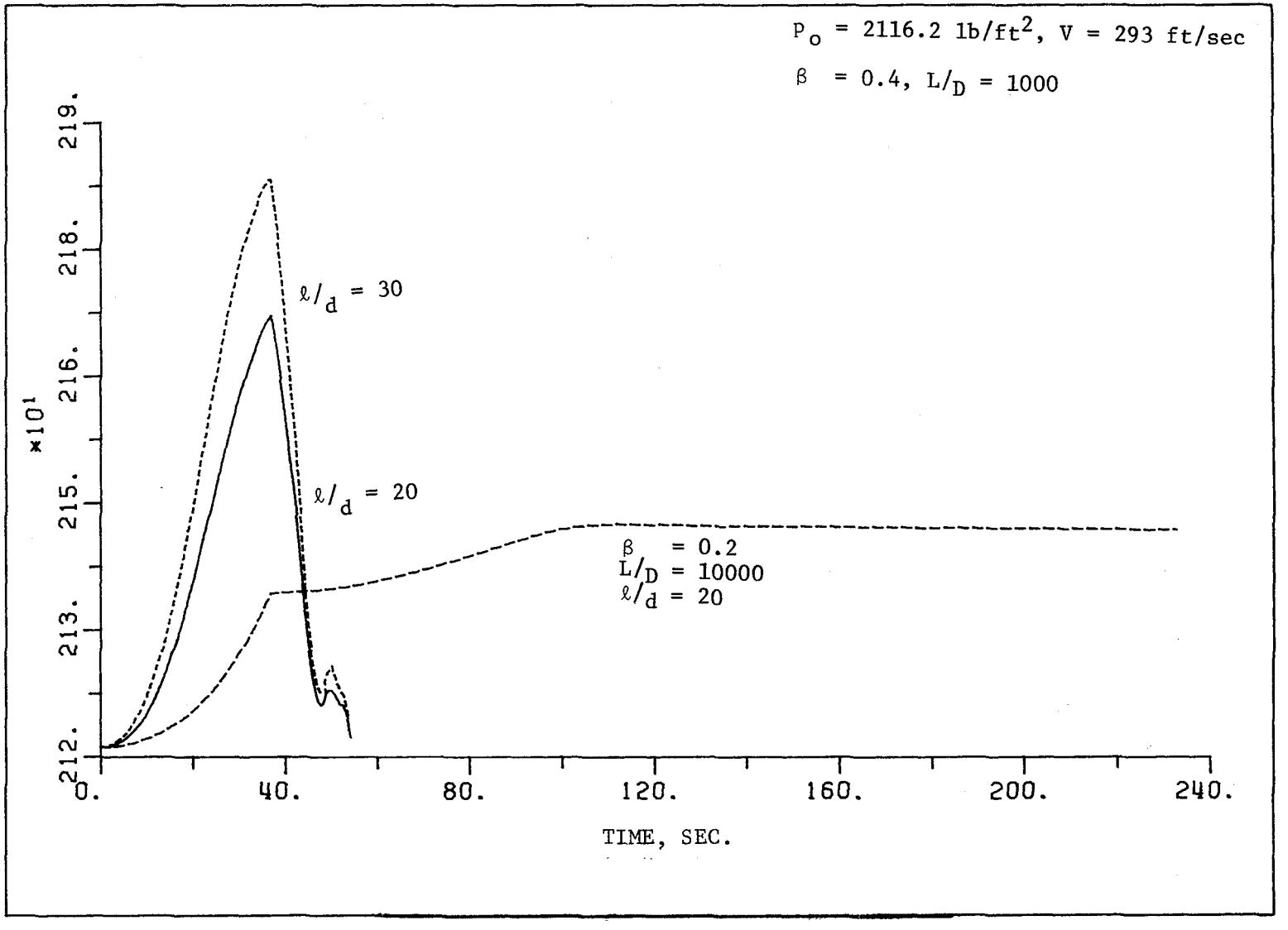

FIGURE 12

PRESSURE AT VEHICLE NOSE, EFFECT OF VEHICLE $\ell/_d$ RATIO

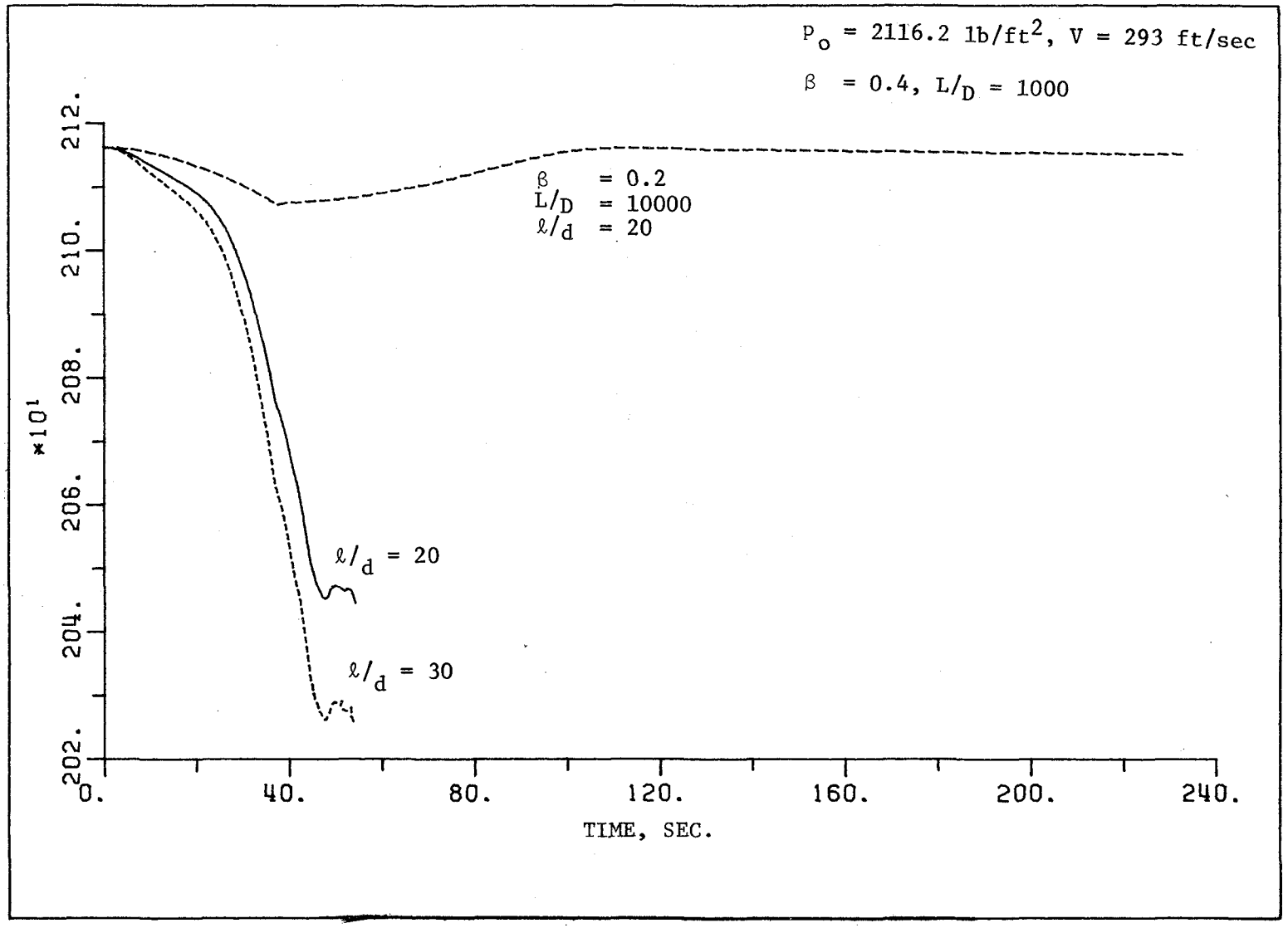

FIGURE 13

PRESSURE AT VEHICLE TAIL, EFFECT
OF VEHICLE $\ell/_d$ RATIO

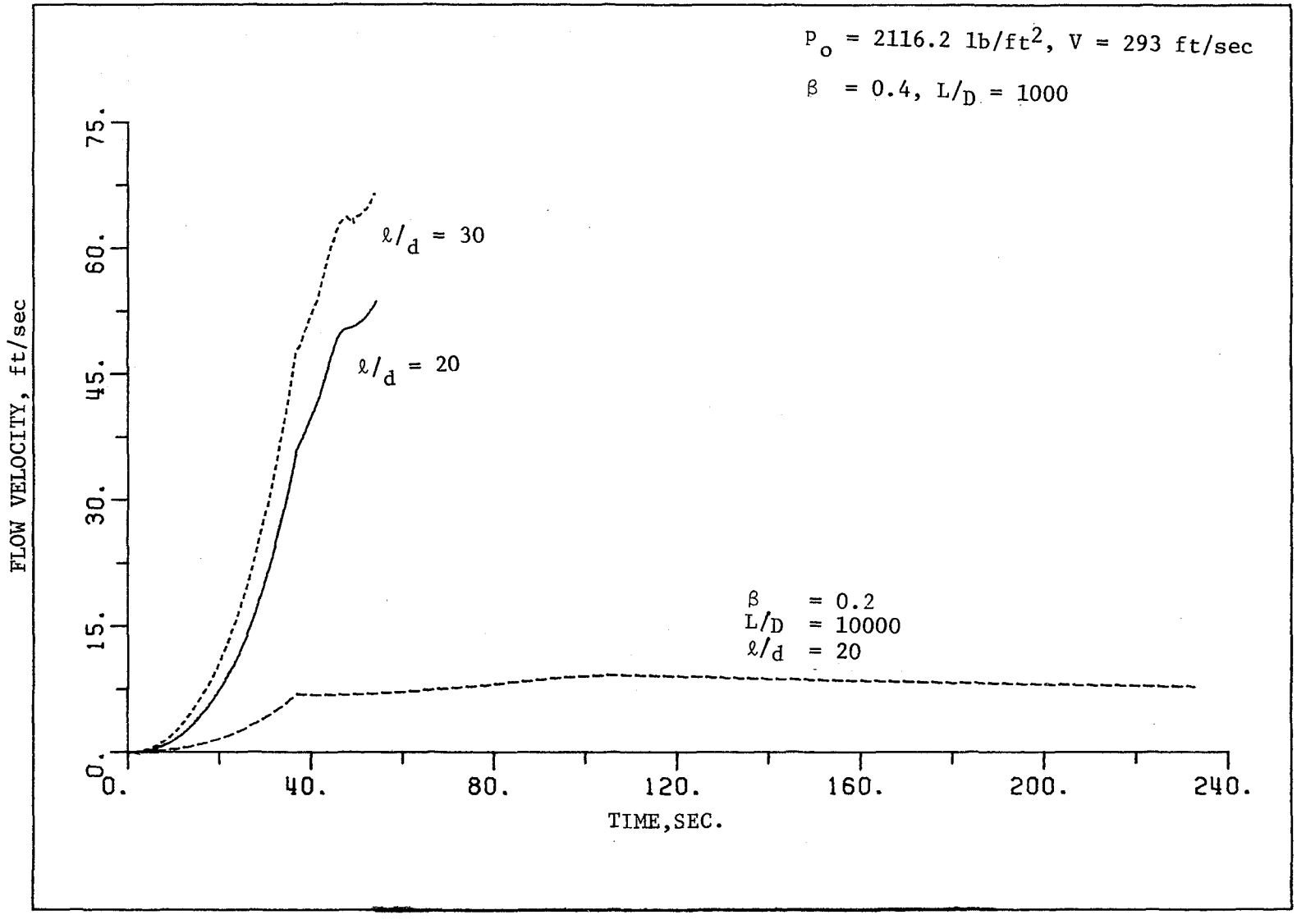

FIGURE 14

FLOW VELOCITY AT VEHICLE NOSE,
EFFECT OF VEHICLE ℓ/d RATIO

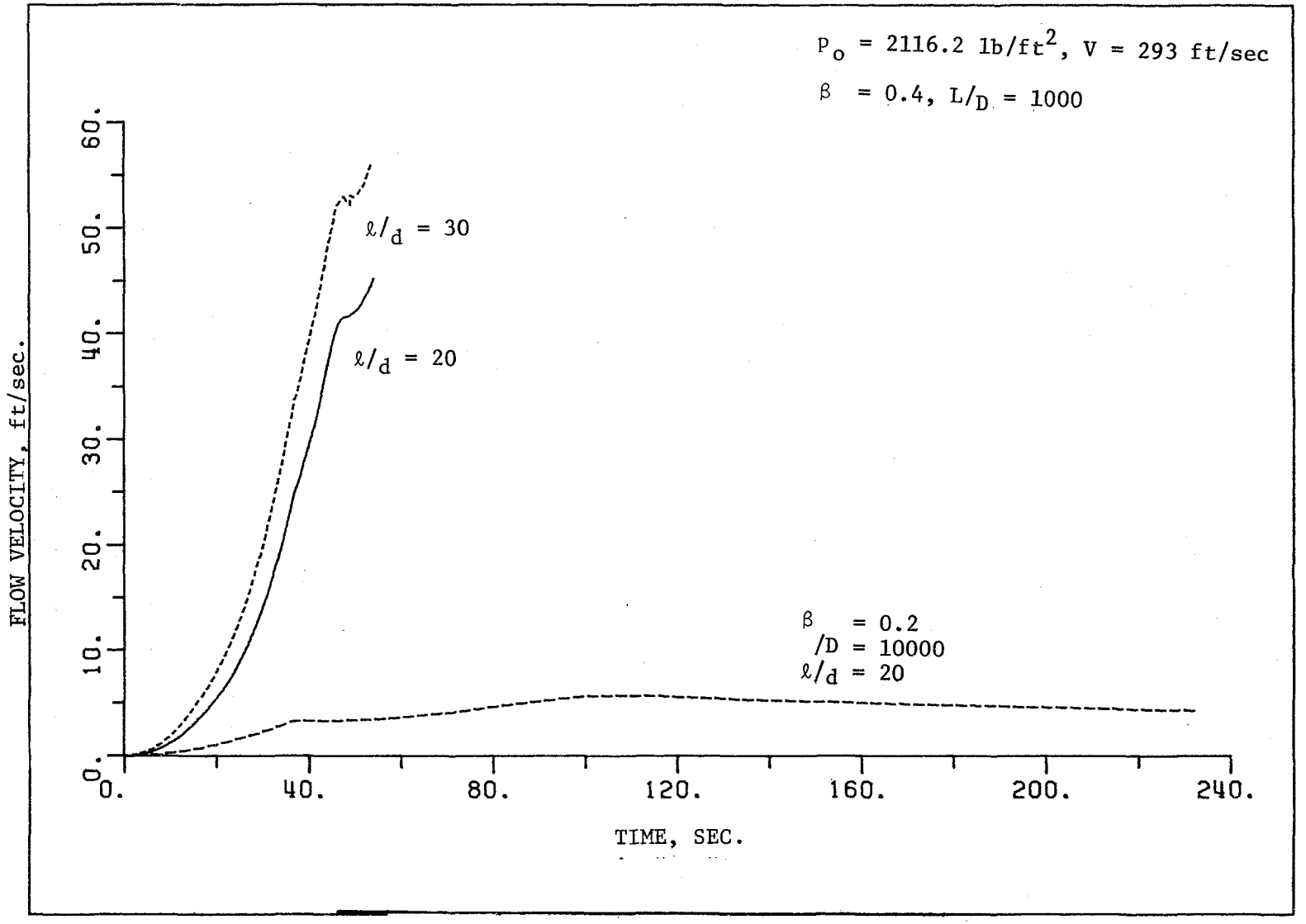

FIGURE 15

FLOW VELOCITY AT VEHICLE TAIL,

EFFECT OF VEHICLE ℓ/d RATIO

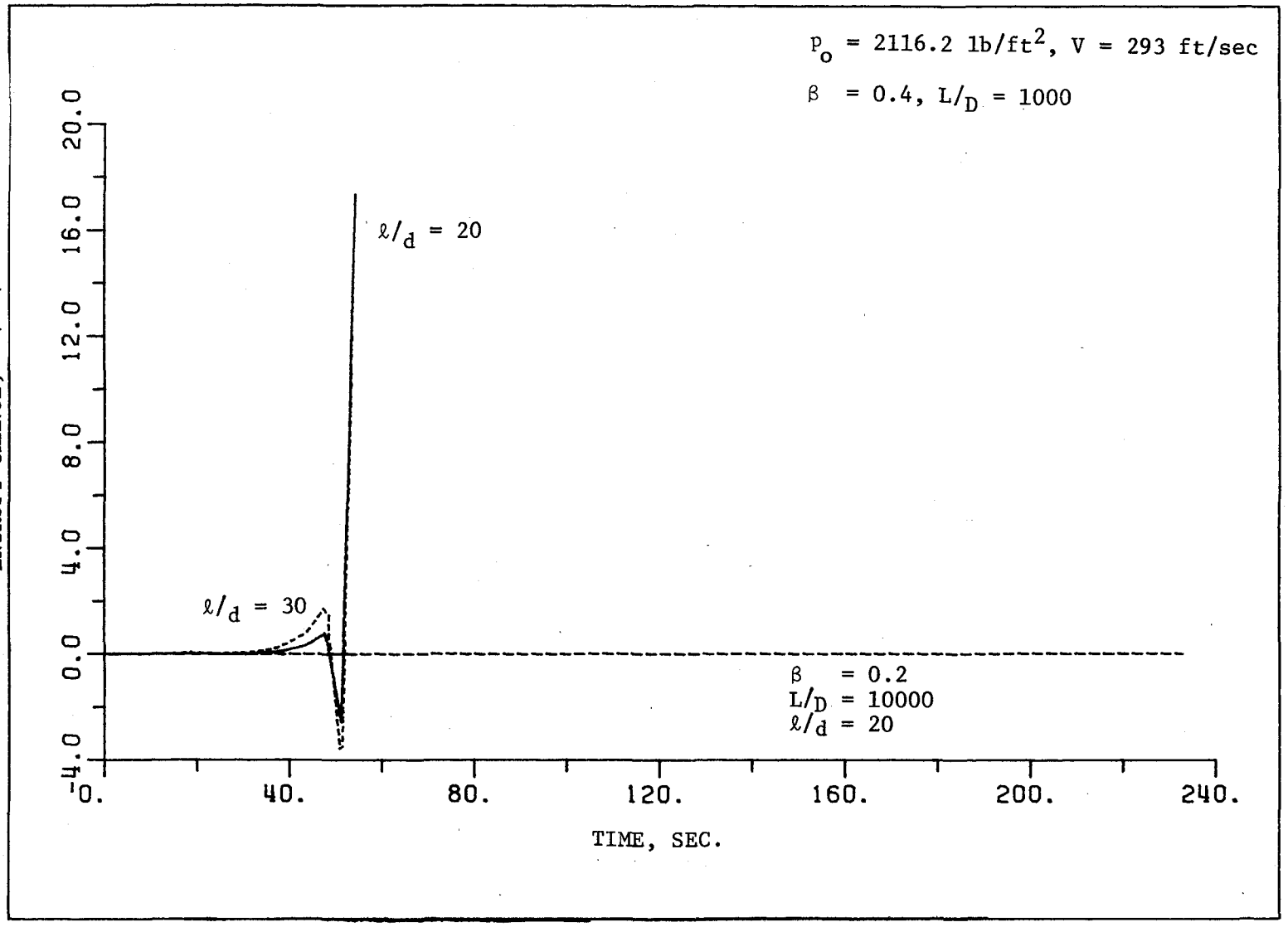

FIGURE 16

ENTROPHY CHANGE OF VEHICLE NOSE,
EFFECT OF VEHICLE ℓ/d RATIO

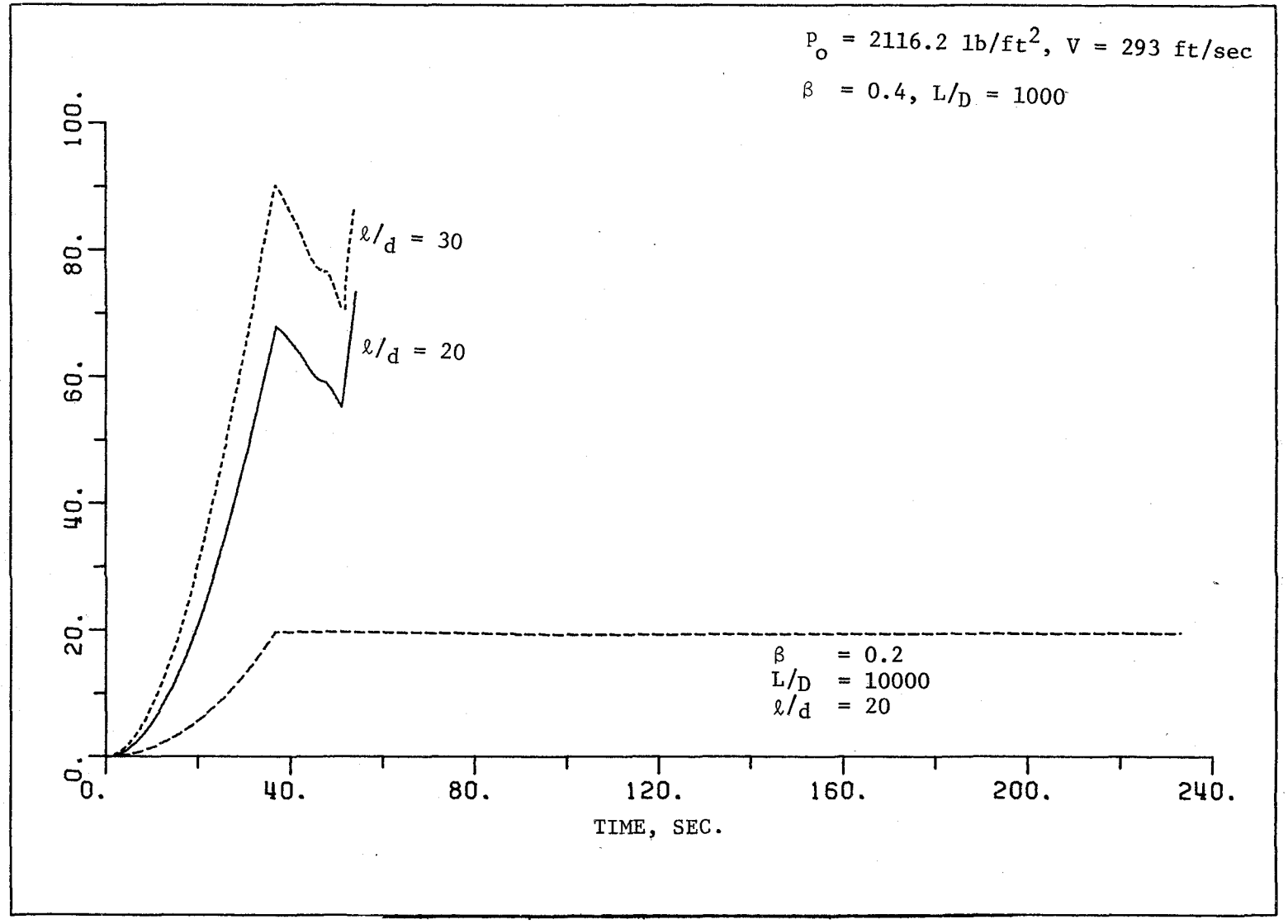

FIGURE 17

ENTROPHY CHANGE AT VEHICLE TAIL,
EFFECT OF VEHICLE ℓ/d RATIO

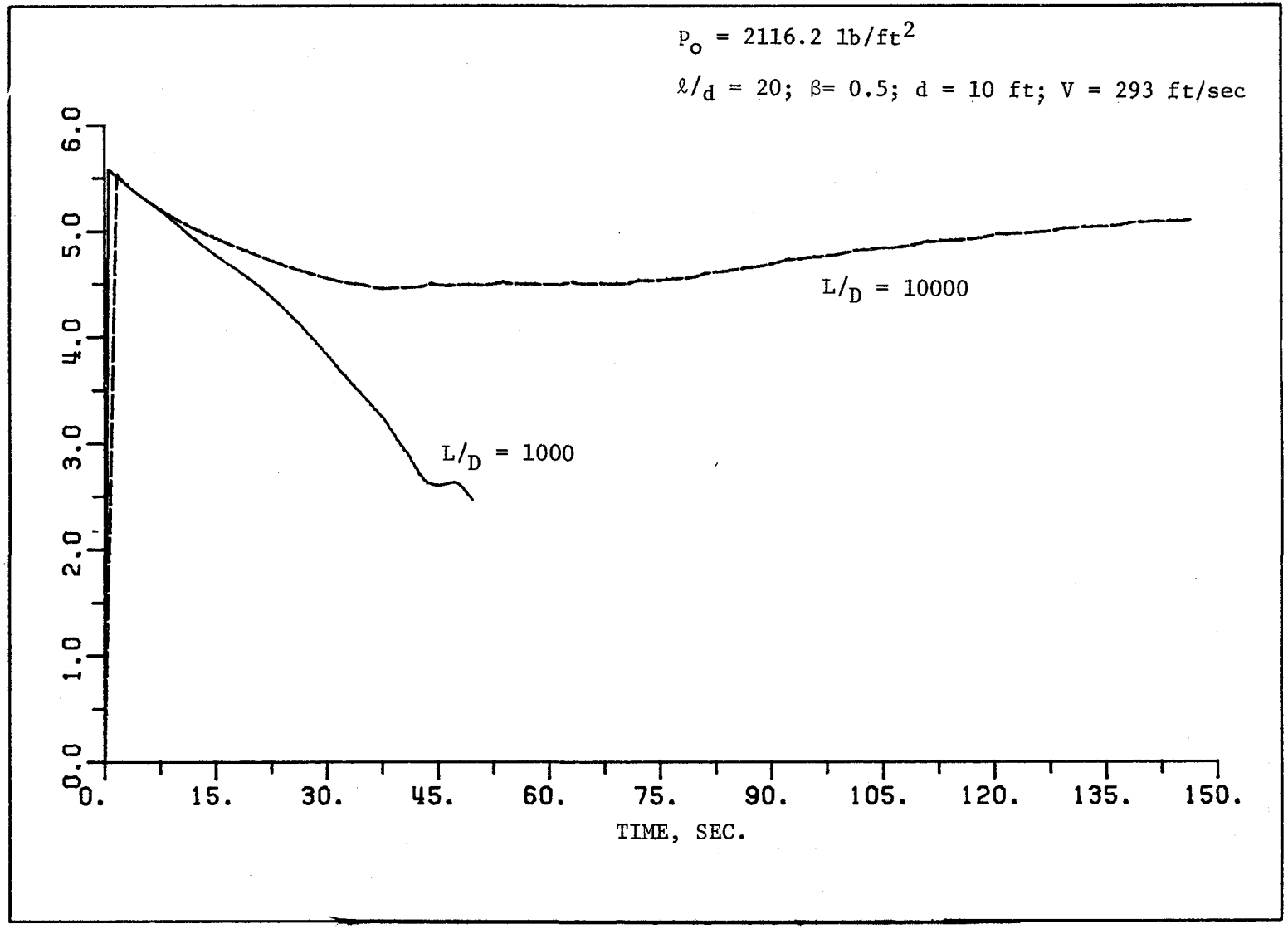

FIGURE 18

DRAG COEFFICIENT AT TIME FOR VARIOUS
TUNNEL L/D RATIOS, OPEN ENDED TUNNEL

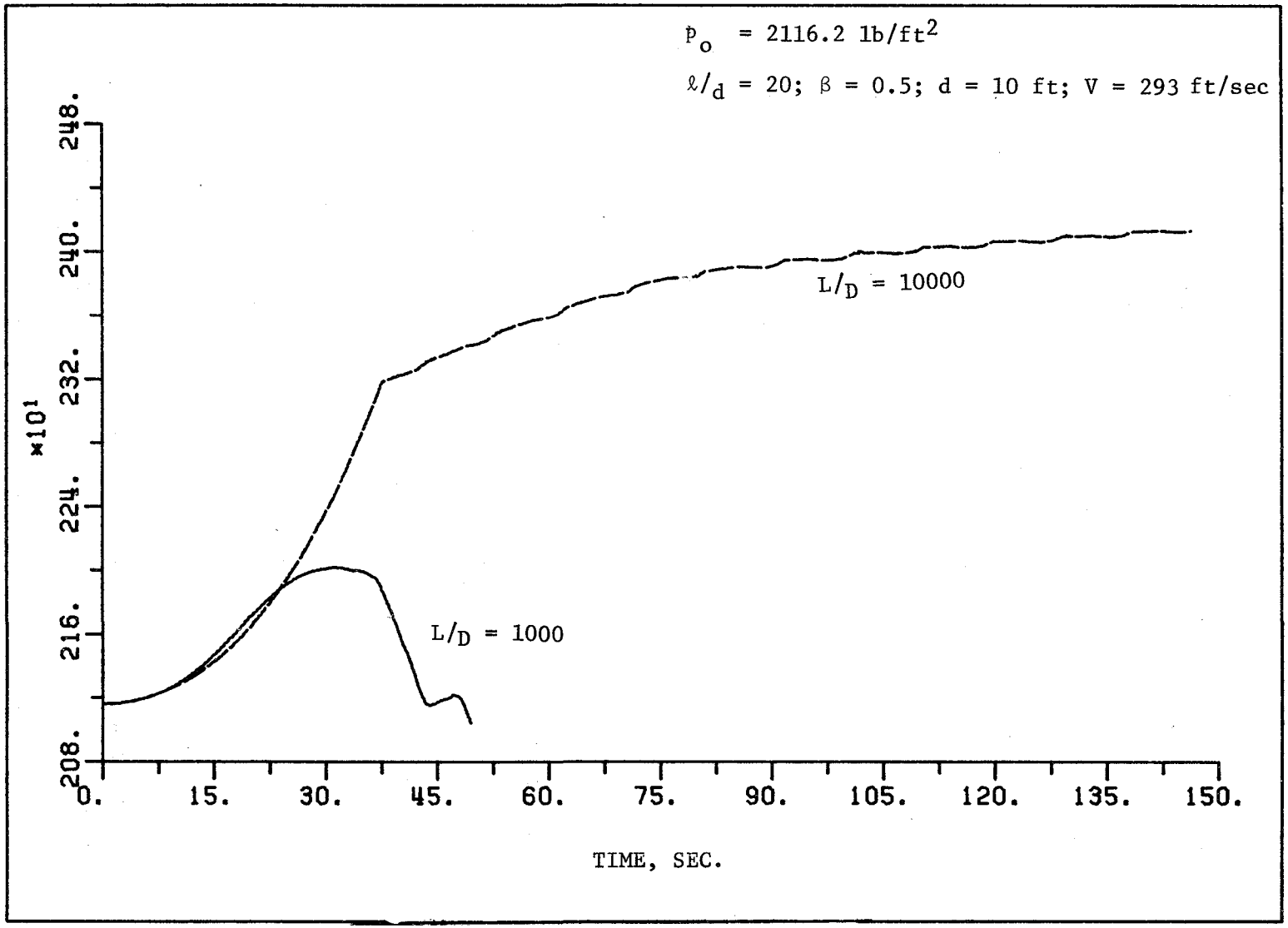

FIGURE 19

PRESSURE AT VEHICLE NOSE, EFFECT OF TUNNEL L/D RATIO

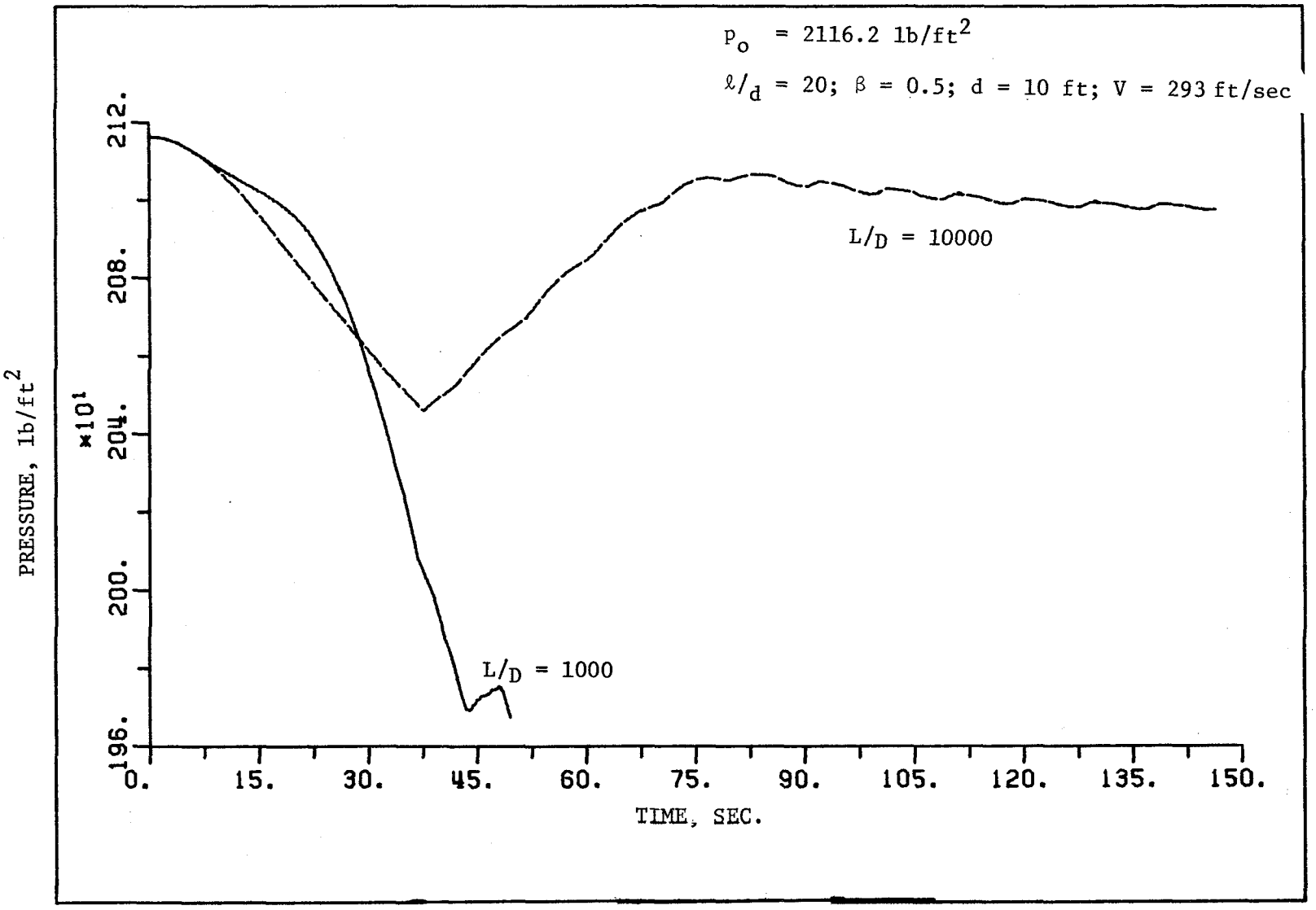

FIGURE 20

PRESSURE AT VEHICLE TAIL, EFFECT OF
TUNNEL L/D RATIO

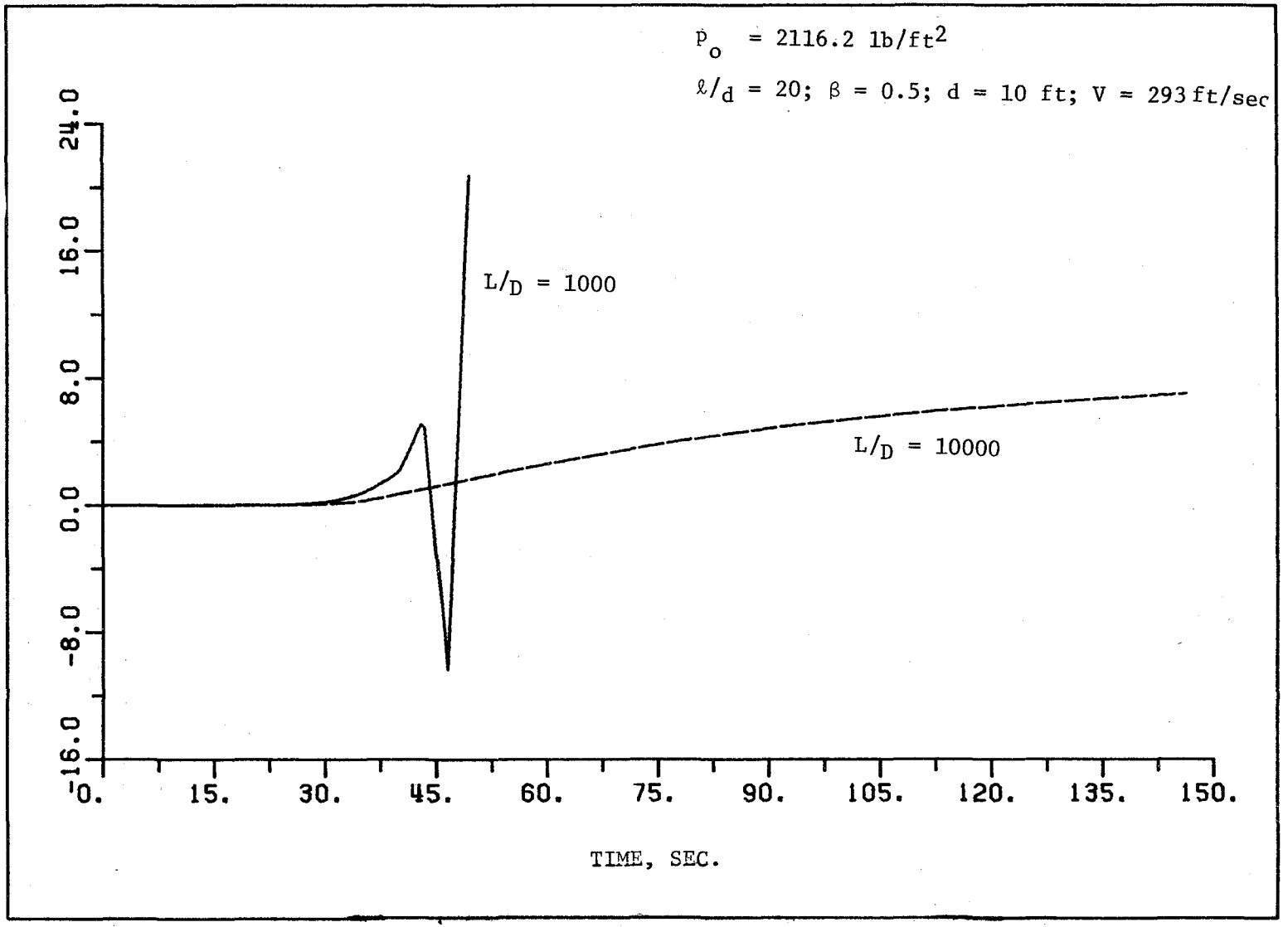

FIGURE 23

ENTROPHY CHANGE AT VEHICLE NOSE, EFFECT
OF TUNNEL L/D RATIO

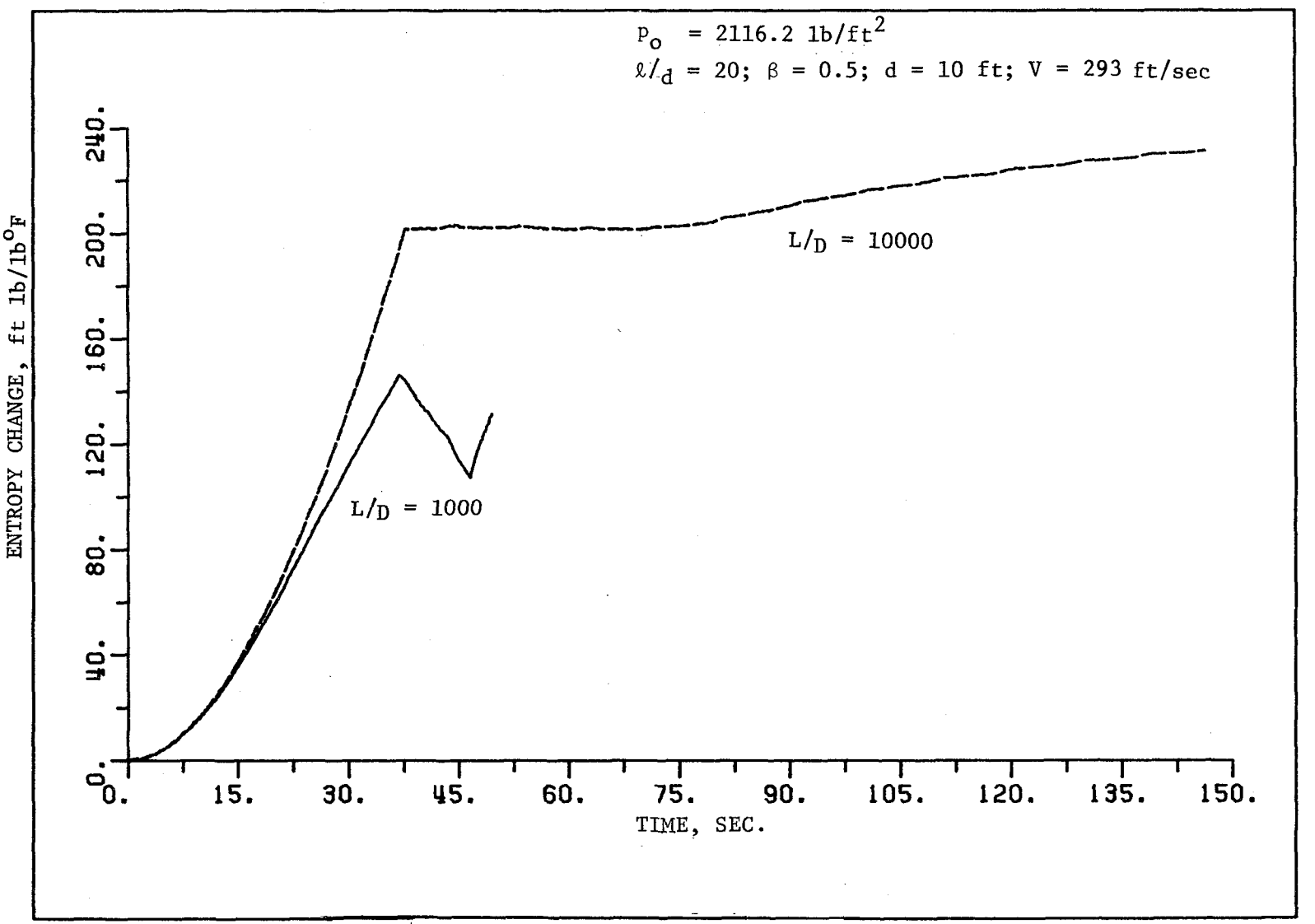

FIGURE 24

ENTROPHY CHANGE AT VEHICLE TAIL, EFFECT
OF TUNNEL L/D RATIO

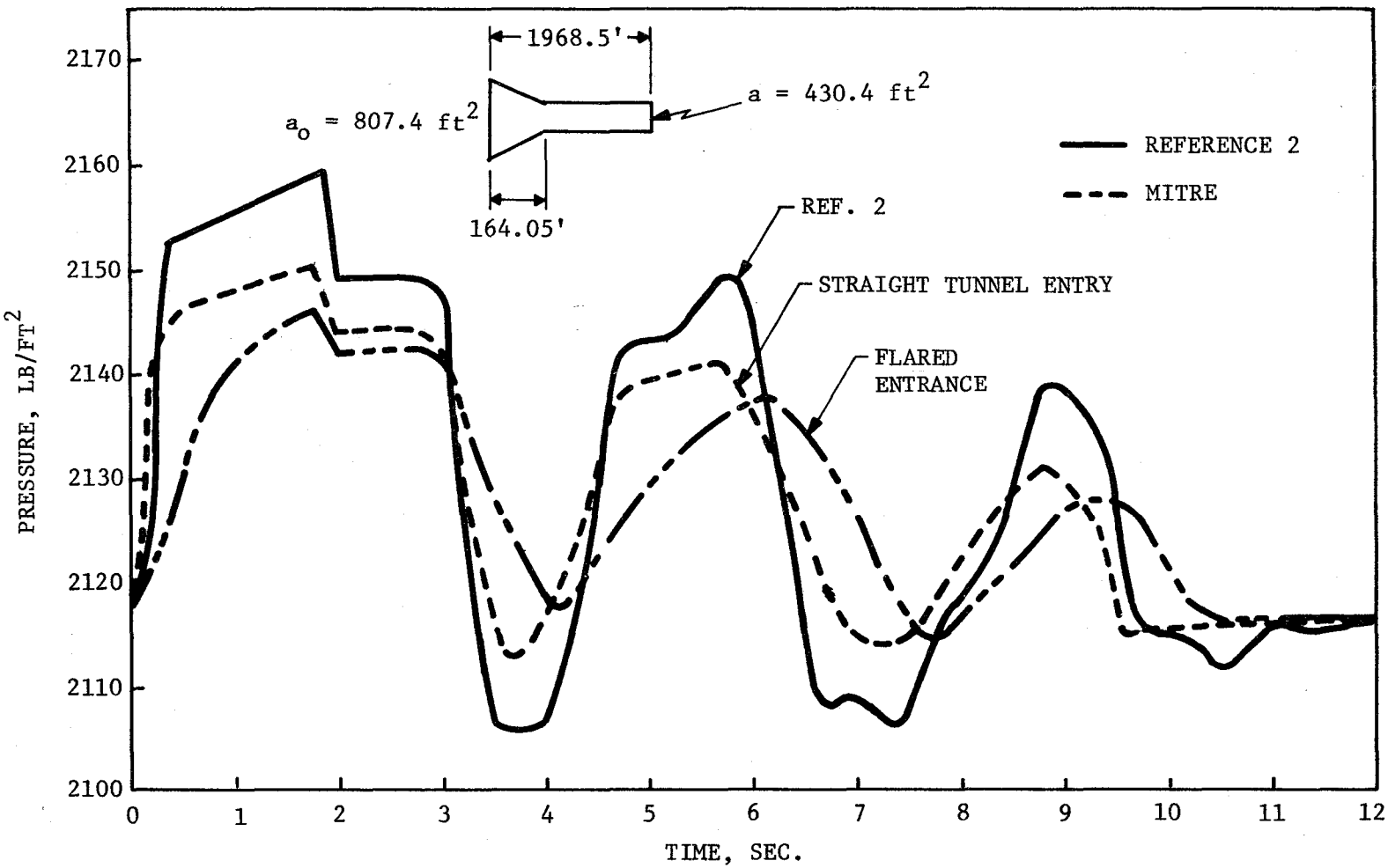

FIGURE 25
PRESSURE IN FRONT OF VEHICLE
TUNNEL ENTRY VELOCITY = 164.04 ft/sec ℓ_v = 246.06 ft; L_T = 1970 ft; β = 0.19

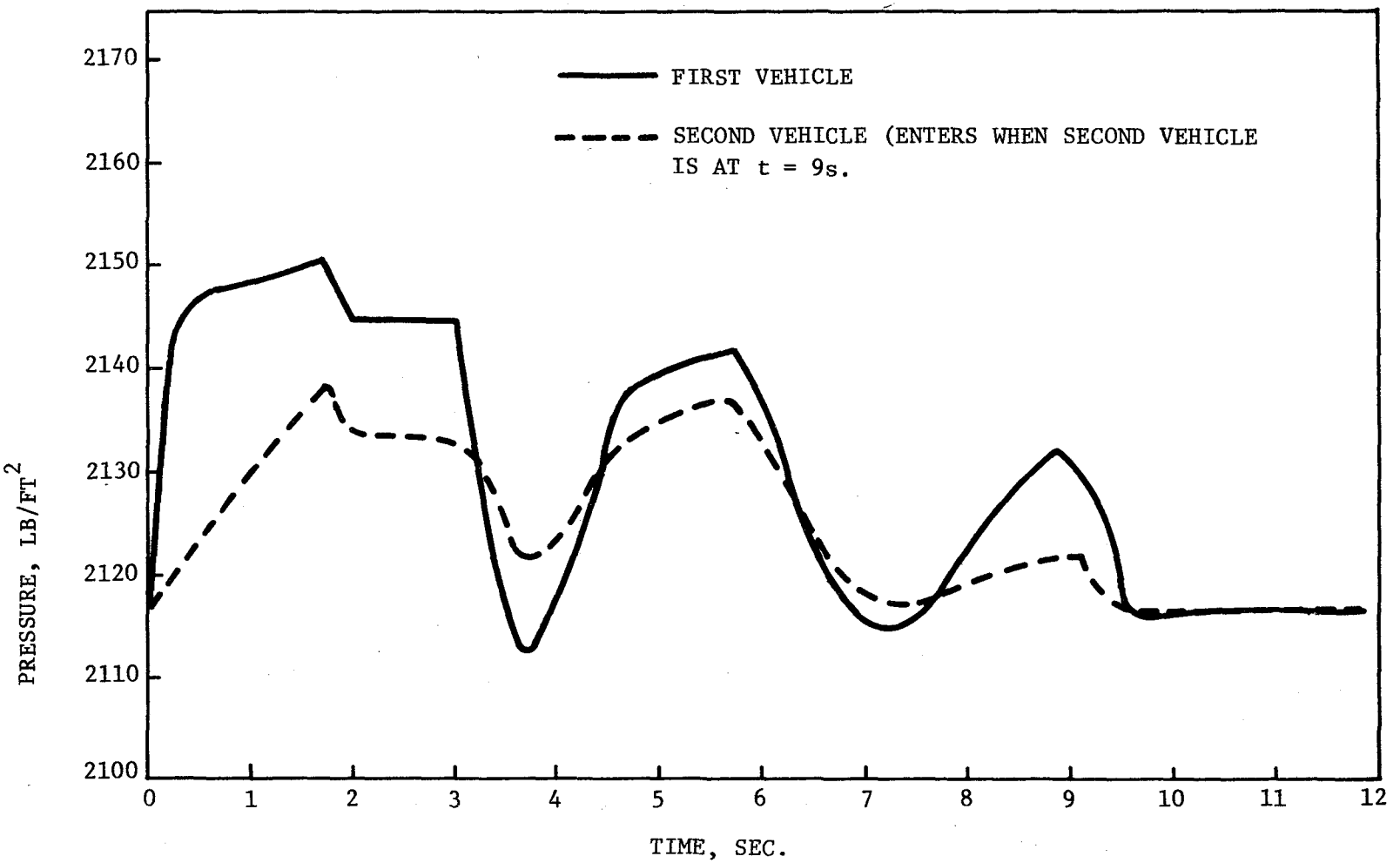

FIGURE 26
PRESSURE IN FRONT OF VEHICLES ENTERING TUNNEL AT SUCCESSIVE INTERVALS
TUNNEL ENTRY VELOCITY = 164.04 ft/sec; ℓ_v = 246.06 ft; ℓ_t = 1970 ft; β = 0.19

B63

59